Editors' Suggestion

Absolute frequency referencing for swept dual-comb spectroscopy with midinfrared quantum cascade lasers

K. N. Komagata [1,*] V. J. Wittwer [1] T. Südmeyer,[1] L. Emmenegger [2] and M. Gianella [2,†]

[1]*Laboratoire Temps-Fréquence, Institut de Physique, Université de Neuchâtel, Avenue de Bellevaux 51, 2000 Neuchâtel, Switzerland*

[2]*Laboratory for Air Pollution / Environmental Technology, Empa, Überlandstrasse 129, 8600 Dübendorf, Switzerland*

(Received 4 August 2022; accepted 9 December 2022; published 26 January 2023)

Quantum cascade laser (QCL) frequency combs have revolutionized midinfrared (MIR) spectroscopy by their high brightness and fast temporal resolution, and are a promising technology for fully integrated and cost-effective sensors. As for other integrated comb sources such as microcombs and interband cascade lasers, QCLs have a comb spacing of several GHz, which is adequate for measurements of wide absorbing structures, typically found in liquid or solid samples. However, high-resolution gas-phase spectra require spectral interleaving and frequency calibration. We developed a frequency calibration scheme for fast interleaved measurements with combs featuring multi-GHz spacing. We then demonstrate dual-comb spectroscopy with a best accuracy of 600 kHz in single-shot 54 ms measurements spanning 40 cm^{-1} (1.2 THz) using QCLs at 7.8 μm (38.4 THz). This work paves the way for unambiguous and fast fingerprinting of complex molecular mixtures in the MIR with integrated comb sources.

DOI: 10.1103/PhysRevResearch.5.013047

I. INTRODUCTION

Over the last two decades, dual-comb spectroscopy [1,2] has developed into a powerful tool for applications requiring fast temporal resolution, high spectral accuracy, and broad spectral coverage. It has enabled difficult or previously impossible measurements, such as multispecies trace gas detection in open path [3], monitoring of irreversible processes with microsecond resolution [4], hyperspectral 3D imaging [5], and fast determination of isotope ratios of multiple species [6]. Moreover, photonic chip integrated comb sources such as microcombs [7], quantum cascade lasers (QCLs) [8], and interband cascade lasers [9] are potential game changers, by enabling mass-producible integrated gas sensors for demanding fields, such as health, security, environment, and industrial process monitoring.

However, these integrated comb sources, due to their small size, have large (compared to fiber mode-locked lasers) repetition rates, f_{rep}, on the order of 10 GHz or higher. The large f_{rep}, while allowing a high temporal resolution, leads to a sparse spectrum, where narrow molecular absorption is potentially lost between the comb teeth.

This limitation is not unique to dual-comb spectroscopy or to integrated comb sources, and has been addressed by interleaving many (up to many thousands) offset spectra, where f_{rep} and/or the offset frequency, f_o, are tuned in steps [10–16] or continuously [17,18].

Step-tuning of referenced combs typically consists of stepping the repetition rate by tens of Hz with dwell times on the order of seconds or more. Thus, the full interleaved spectrum is acquired in tens or hundreds of seconds and the frequency accuracy is that of the static comb [12,15]. We note that step-tuning was also used with free running midinfrared (MIR) QCLs, where a full spectrum was obtained in 1200 s with an accuracy better than 12 MHz [16]. Continuous sweeps yield faster measurements with higher spectral point density. However, they require an adapted frequency calibration scheme. The endless frequency comb was proposed by Benkler *et al.* [19], but it is not convenient in the MIR as it requires electro-optic components and pulsed emission. Alternatively, the use of an unbalanced Mach-Zehnder interferometer provided frequency scales with 10 MHz level precision for NIR microcombs [18] and MIR QCLs [20], with sweep times of 50 μs and 30 ms, respectively.

In this work, we present a method to calibrate fast continuous sweeps of multi-GHz frequency combs with sub-MHz accuracy, which can be applied independently of the wavelength range. We thus demonstrate a QCL-based MIR dual-comb spectrometer with a unique combination of fast acquisition, high-frequency accuracy, and high spectral point density.

As a proof of concept, we measure 43 transitions of the ν_1 rovibrational band of N_2O and 56 transitions belonging to the ν_4 band of CH_4. With the former measurement, we characterize the accuracy of the computed frequency scale and assess the precision of the measurement at varying scanning speeds. The latter provides an independent measurement of the transition frequencies of CH_4 which were recently published [21].

Rapid scanning and high accuracy are critical features for fingerprinting of complex molecular mixtures and parallel

*Corresponding author: kenichi.komagata@unine.ch

†Present address: IRsweep AG, Laubisrütistrasse 44, 8712 Stäfa, Switzerland.

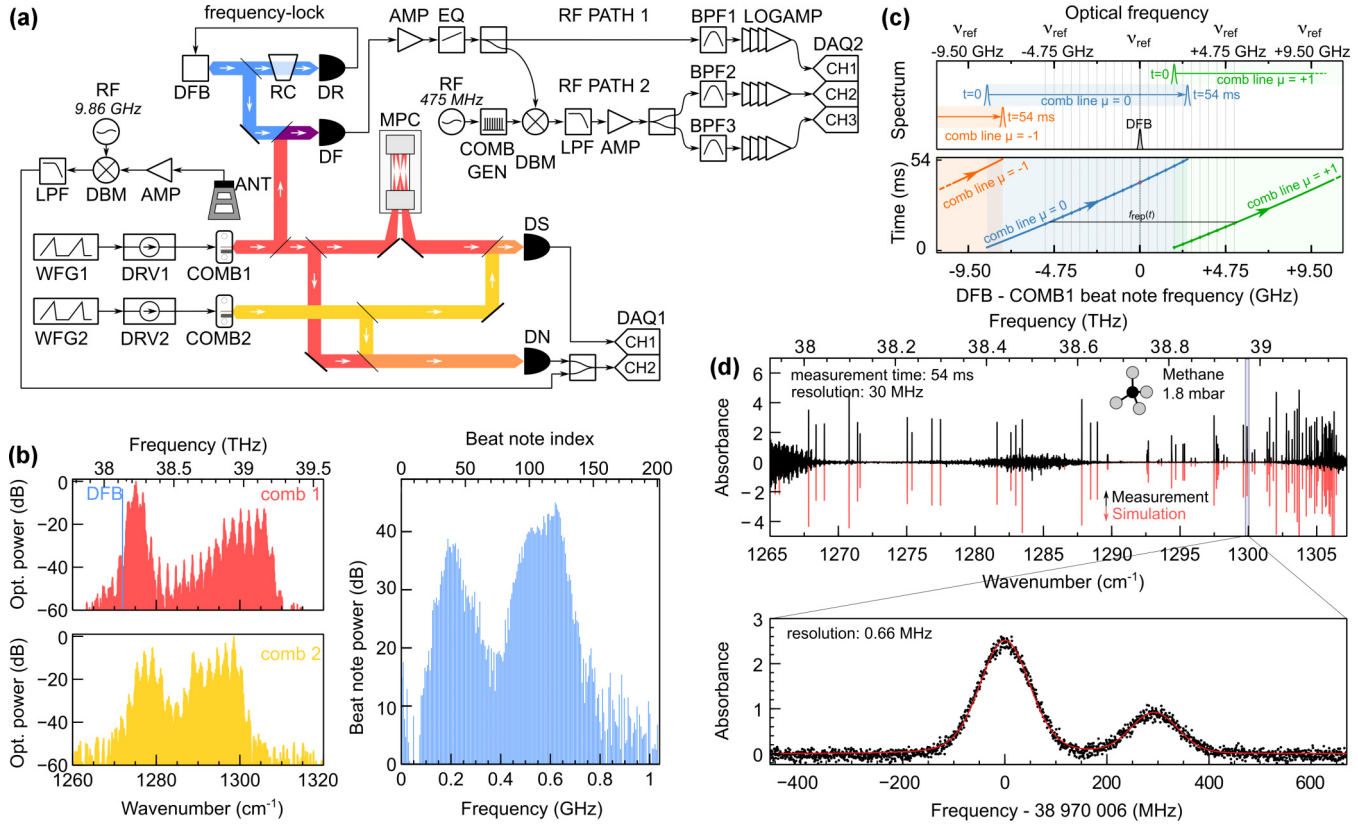

FIG. 1. Experimental setup and schematic for accurate frequency scale. (a) Experimental setup featuring the distributed feedback (DFB) laser serving as frequency reference, the gapless dual comb spectrometer, and the setups to measure the repetition rate and the optical frequency during an acquisition. MPC: multipass cell, AMP: amplifier, BPF, LPF: bandpass (low-pass) filter, DBM: double-balanced mixer, LOGAMP: logarithmic amplifier, EQ: equalizer, COMB GEN: comb generator, WFG: wave form generator, DAQ: data acquisition unit, DS, DN, DR, DF: photodetector (see main text). (b) Optical spectra of COMB1, COMB2, the position of the reference DFB laser, and the multi-heterodyne beat spectrum. (c) Schematic of the referencing scheme of the optical frequencies of COMB1 while they are tuned across more than one free-spectral range (f_{rep}), relying on the use of a synthetic comb. (d) Absorption spectrum of low-pressure methane acquired in 54 ms by our spectrometer. The top panel is digitally filtered for visibility while the lower panel features two absorption lines at the original resolution of 660 kHz.

frequency modulated lidar [22]. Accordingly, we trust that our enhanced method for frequency axis calibration is a highly valuable asset for ranging and MIR sensing.

II. SPECTROMETER DESCRIPTION

Our dual-comb spectrometer is composed of two QCL frequency combs (COMB1 and COMB2), similarly to a previous work [17], and is schematized in Fig. 1(a). COMB1 is the interrogating comb which probes the sample contained in a multipass cell, and COMB2 is the local oscillator. The repetition frequency of the combs, $f_{\mathrm{rep}} \approx 9.88$ GHz, is too large to sample Doppler-broadened gas-phase spectra of small molecules. Therefore, we tune the driving current to scan the comb lines across f_{rep} and interleave spectra to reduce the spectral point spacing by 4 orders of magnitude. The local oscillator comb is tuned synchronously to keep the multi-heterodyne spectrum within the detection bandwidth of the system [see Fig. 1(b)]. The interferograms measured on the photodetectors DS and DN are divided into slices of length $\tau = 13.1$ μs, which are sufficiently long to resolve the beat notes (beat note spacing, $\Delta f_{\mathrm{rep}} \approx 4.5$ MHz). A lower limit for the spectral resolution, $\delta\nu$, can be estimated from the effective slice length, $\tau/3.77$, and the tuning rate, $\dot{\nu}$,

$$\delta\nu = \dot{\nu}(\tau/3.77). \tag{1}$$

The employed flat-top apodization reduces the effective length of the slice by a factor of 3.77. For example, the spectrometer can acquire spectra spanning 40 cm^{-1} (1.2 THz) in 54 ms at a point spacing and resolution of 0.66 MHz, allowing measurement of low-pressure methane [see Fig. 1(d)]. The noise-equivalent absorbance and noise-equivalent absorption coefficient depend on the signal-to-noise ratio (SNR) of the corresponding beat note [see Fig. 1(b)]. For strong beat notes, they are of the order of 3×10^{-4} $\mathrm{Hz}^{-1/2}$ and 8×10^{-8} cm^{-1} $\mathrm{Hz}^{-1/2}$, respectively, given the absorption path length of 36 m in the multipass cell.

The distributed feedback QCL (DFB) is locked to a molecular transition [N_2O, fundamental ν_1 band, P(14)] via wavelength modulation spectroscopy and acts as an optical frequency reference with frequency ν_{ref} [23]. The beat frequency, f_b, between the reference laser and COMB1 is detected on a 1.2 GHz bandwidth detector (DF). The frequency, $\nu_\mu(t)$, of all lines, $\mu = 0, \pm1, \pm2, \ldots$, of the interrogating

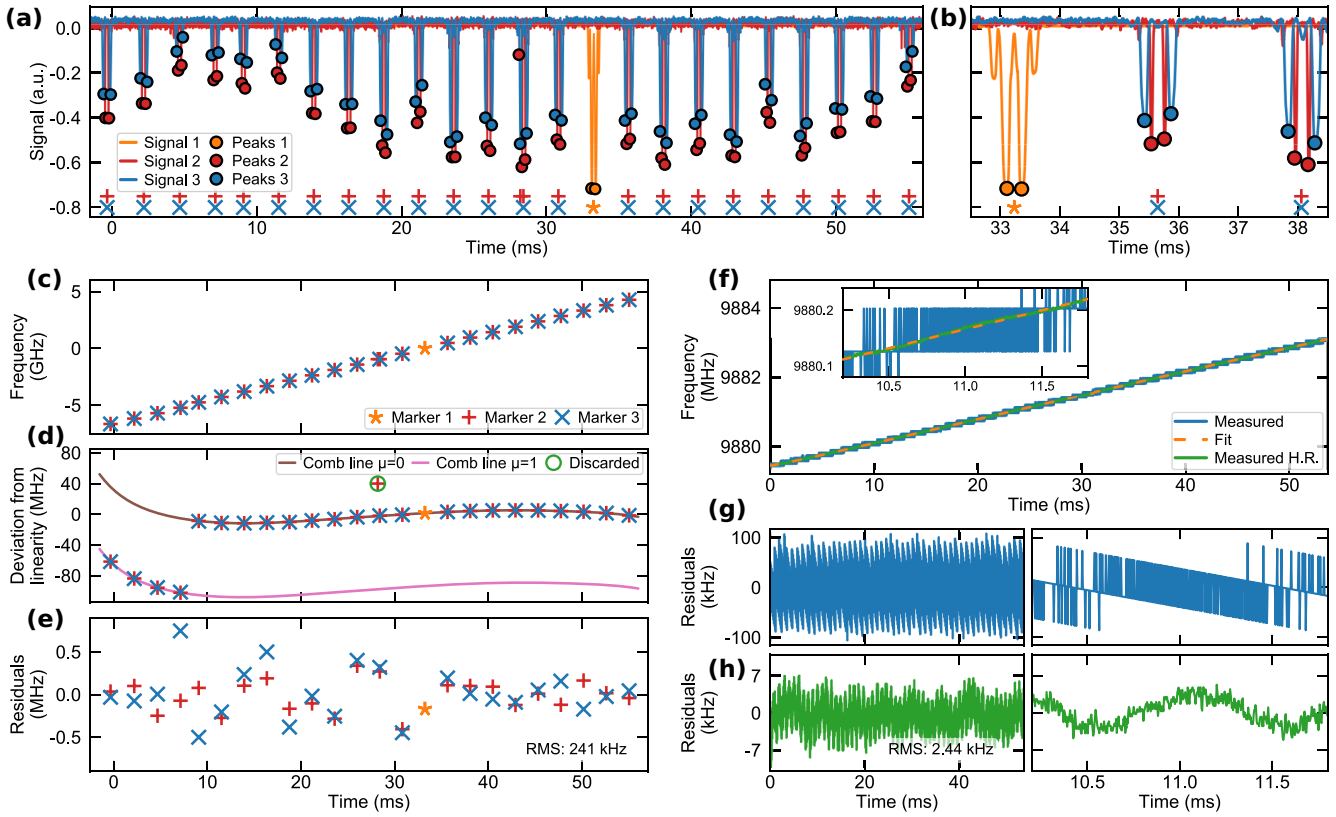

FIG. 2. Assessment of f_b and $f_{\rm rep}$ over a gapless measurement (sweep range $\geqslant f_{\rm rep}$). (a) Filtered marker signal digitized by DAQ2 [see Fig. 1(a)] as a function of time (solid lines) and pulses localized by the algorithm (filled circles). The mean position of two pulses gives the marker position shown by a star, plus, or x. (b) Zoom over 3 pairs of pulses. (c) Frequency of the markers as a function of time. (d) Frequency of the markers minus the linear trend and polynomial fitting of the comb line frequency. The first 4 pairs of marker originate from the beat with another comb line ($\mu = 1$ instead of $\mu = 0$). (e) Residuals from the fit from (d). (f) Measured $f_{\rm rep}$ using two methods as a function of time and fit. The inset shows the a zoom over a smaller time interval. (g), (h) Residuals of $f_{\rm rep}$ measured through the fast processor (g), which is limited by the integration time, or measured with high resolution (H.R.) (h). The right plot shows a zoom over a smaller interval. The fit using the processor data is accurate for the H.R. data within 2.4 kHz.

comb over the time of the scan is computed from the measured repetition rate, $f_{\rm rep}(t)$, and beat frequency, $f_b(t)$, at each slice of the sweep, and is given by

$$\nu_\mu(t) = \nu_{\rm ref} + f_b(t) + \mu f_{\rm rep}(t). \tag{2}$$

III. EVALUATION OF THE FREQUENCY AXIS

Thus, the reconstruction of the frequency axis of the interleaved spectra requires accurate knowledge of $f_b(t)$ and $f_{\rm rep}(t)$ at each slice of the sweep. An approach to determine $f_b(t)$ and $f_{\rm rep}(t)$ would be to measure and digitize them before applying a Fourier transform with a moving window. However, this is not a satisfying solution for $f_b(t)$ as it requires a costly high-speed digitizer and a custom or nitrogen-cooled detector that accommodates the sweeps of $f_b(t)$ over the large RF bandwidth of 5 GHz (corresponding to $f_{\rm rep}/2$). Besides the costs, that approach necessitates the storage and processing (Fourier transform) of large data sets, which are already demanded supplies for the processing of the dual-comb interferogram and especially needed for QCL-based dual combs [24].

We therefore apply another approach for the measurement of $f_b(t)$, based on the open-loop solution proposed in 2009 by Del'Haye *et al.* [25] with a few notable changes. Here, the reference laser is fixed while the comb is swept by approximately $f_{\rm rep}$. Therefore, a single pair of peaks is detected through RF path 1 [see Fig. 1(a)], which is not sufficient to calibrate the entire sweep. These are observed at the instants when the bandpass filter BPF1 transmits the beat to the rectifying logarithmic amplifier (LOGAMP). The recorded signal on channel 1 of DAQ2 is shown in Figs. 2(a) and 2(b) as signal 1.

To increment the number of frequency markers, we implement a second RF path [RF path 2; see Fig. 1(a)], where we mix the beat with an $f_{\rm RF} = 475$ MHz spaced harmonic RF comb. The RF comb provides a synthetic grid of frequencies centered on the reference laser frequency, $\nu_{\rm ref}$, and having a spacing of $f_{\rm RF}$ [see Fig. 1(c)], whereby the time of passage of ν_0 across each grid line is measured. Hence, the determination of $f_b(t)$ [or $\nu_0(t)$] is based on the measurement of the times at which f_b equals multiples of $f_{\rm RF}$. These markers allow us to map the frequency of $f_b(t)$ [or $\nu_0(t)$] versus time, as shown in Fig. 2(c). The marker on channel 1 allows identification of $\nu_0(t_0)$ modulo $f_{\rm rep}$.

However, the large RF bandwidth required to measure f_b throughout the sweep still poses a challenge, as the specified

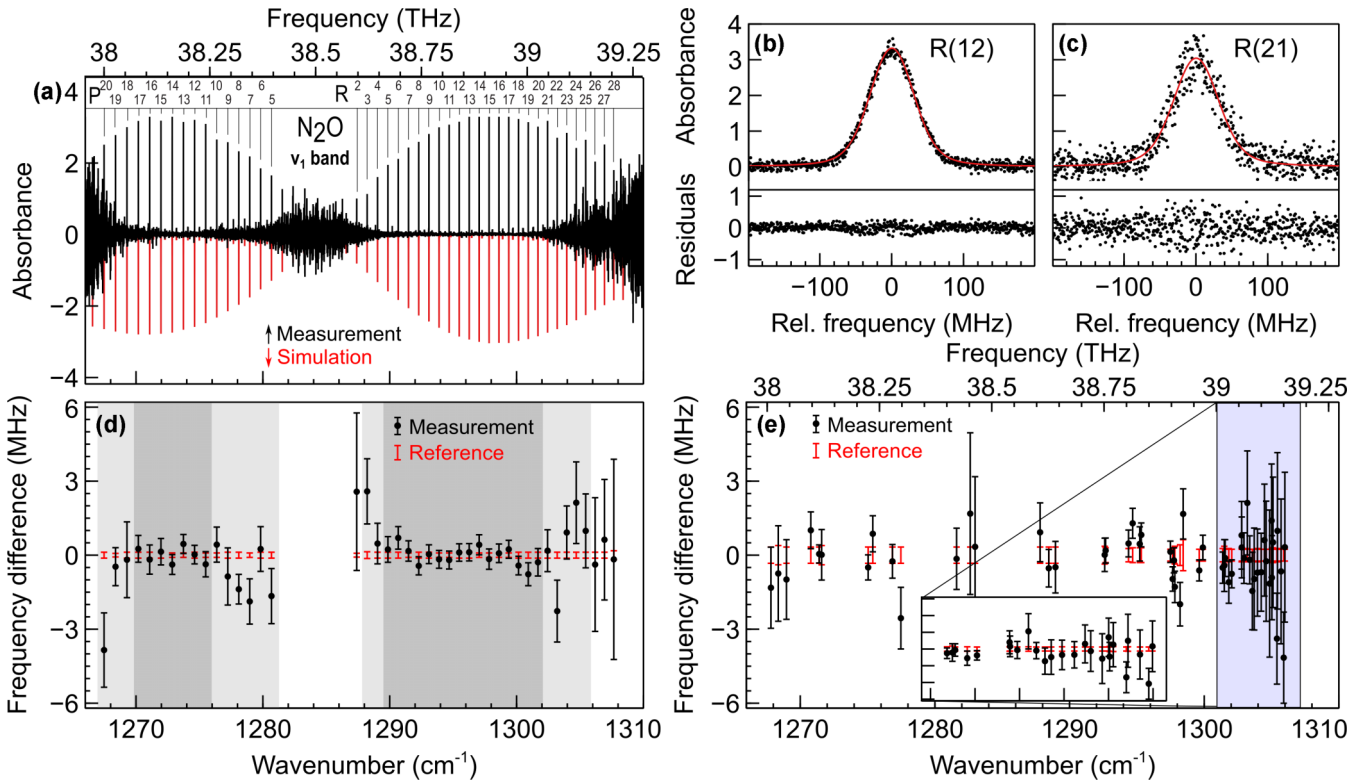

FIG. 3. Single-shot spectra of N_2O and retrieved line centers of N_2O and CH_4 (a) Single-shot spectra of the ν_1 fundamental band of nitrous oxide with 660 kHz spectral point spacing, acquired in 54 ms and comparison with simulation. (b), (c) Zoom of (a) on two different lines illustrating high/low SNR, and residuals of the Voigt fit (shown in red). (d) Retrieved line centers from (a) compared with literature reference [15,27] with the total 1 σ uncertainty shown as the error bars. The dark (light) gray regions depict the frequency ranges where the accuracy is better than 0.6 MHz (2 MHz). (e) Same as (d) for CH_4 averaged over 15 acquisitions, where the reference is taken from Ref. [21]. A zoom over the congested region (blue shading) is shown in the inset.

bandwidth of the photodetector is only 1.2 GHz. We thus used logarithmic amplifiers to increase the marker detection dynamic range and gain equalizers (EQ) to reduce signal strength imbalances. Moreover, in order to further balance the signal strength and optimize the RF mixers, the signals were split below and above 3.8 GHz [not shown in Fig. 1(c)]. Further information can be found in the Appendix and in Note 1 of the Supplemental Material [26].

These adaptations enabled the retrieval of frequency-equidistant markers over the entire sweep [see Fig. 2(c)], determined by the pairs of peaks in signals 2 and 3. We plot the markers after removal of the linear trend in Fig. 2(d). The first 4 sets of markers originate from the beating with a higher comb line $\mu = 1$ [see Fig. 1(c)], which was unavoidable to accommodate a sweep about 10% larger than f_{rep}. We fit the markers with a 10th-order polynomial using a two comb line model separated by $f_{\mathrm{rep}}(t)$. The algorithm is robust against spurious peaks, which produce markers that can be discarded if they do not fit within a certain tolerance region. The residuals of the fit are shown in Fig. 2(e). The standard deviation of the fit residuals is found to be 241 kHz, which is useful for assessing the quality of the fit and for estimating the uncertainties of the adapted marker scheme in this implementation. The polynomial order was chosen to reduce the fit residuals while avoiding the overfitting of the sets of markers numbering to approximately 20.

The repetition rate, detected by the horn antenna, is down-mixed to ∼20 MHz, digitized on DAQ1, channel 2, and processed together with the interferogram [see Fig. 1(a)]. The resolution is limited to 76 kHz due to the finite length ($\tau = 13.1$ µs) of the slices [see Fig. 2(f)]. We fit these data using a 10th-order polynomial. The residuals are limited by the resolution as shown in Figs. 2(g) and 2(h). On a control measurement, we recorded the raw digitized data from DAQ1, channel 2, and computed $f_{\mathrm{rep}}(t)$ with higher resolution by taking longer slices for the Fourier transform. The residuals between the fit from the low-resolution data and the high-resolution data are shown in Fig. 2(h), showing correspondence within 2.4 kHz. The high-resolution data feature oscillations of f_{rep} due to back-reflection from the photodetectors back to COMB1. The period is close to those originating from the limited resolution. The fringes hinder the in-depth study of the optimal polynomial order for the fitting.

IV. RETRIEVED LINE CENTER ACCURACY

Figure 3(a) shows a spectrum of the fundamental ν_1 band of nitrous oxide acquired in a single sweep of 54 ms. The bimodal comb amplitude distribution gives rise to a variable SNR across the spectrum, as can be seen in Figs. 3(b) and 3(c). We used a Voigt fit with fixed Gaussian width (for each transition) to retrieve the line centers of the molecular transitions.

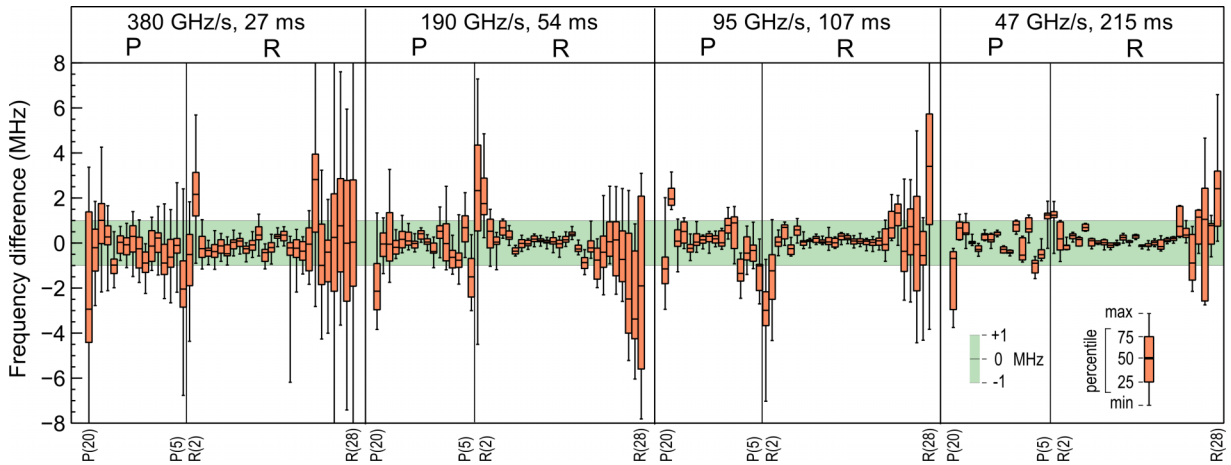

FIG. 4. Frequency precision for varying scanning speed. Statistical spread of the retrieved line centers compared with literature values at 4 different scan speeds, decreasing from left to right by factors of 2. The precision increases with the scan time.

The line centers were then corrected for zero pressure by subtracting the estimated pressure-induced shift.

We benchmark the frequency accuracy of our spectrometer by comparing the computed line center frequencies to those obtained by two other groups with a 100 kHz level accuracy [15,27]. Based on multiple sets of measurements over the course of a few weeks, we estimate that we retrieve, in a single-shot acquisition, 40 line centers [spanning 30.4 cm^{-1} (911 GHz)] with a 1 σ accuracy better than 2 MHz, among which 23 lines [spanning 17.1 cm^{-1} (513 GHz)] are retrieved with an accuracy better than 0.6 MHz, as can be seen in Fig. 3(d).

This estimation includes the uncertainties of the reference laser frequency ν_{ref} [180 kHz after correction of a systematic bias of (180 ± 100) kHz], f_{rep} [2.6 kHz after the correction of a systematic bias of (2.9 ± 0.7) kHz], the fit of the markers as in Fig. 2(e) (240 kHz), and the standard deviation of the retrieved line center frequencies over 12 consecutive 54 ms measurements (below 300 kHz for the lines with the best SNR; see Fig. 4). The retrieved line centers and the uncertainties are consistent with the literature values. The uncertainty on ν_{ref} includes type B uncertainties stemming from the literature value of the reference transition (72 kHz [27]) and from the frequency offset between the lock point and the center of the transitions (130 kHz [23]). All other uncertainties are of type A, including those on the biases. The biases and their uncertainties were computed by comparing our measured N_2O transition frequencies to the literature values.

The frequency accuracy of the spectrometer allows us to retrieve the line centers of CH_4 with a higher accuracy than in the HITRAN database [28]. Our results are given in Table 1 of the Supplemental Material [26]. For this measurement, we averaged the retrieved line centers over 15 measurements. In Fig. 3(e), we compare our results with the recent data published in Ref. [21]. We observe consistency between the results, considering the 1 σ uncertainty. Their spectrometer granted a higher-frequency accuracy while requiring acquisition times of hundreds of seconds for a full interleaved spectrum. We note that we applied the biases determined from the N_2O measurement.

V. SCANNING SPEED

The scanning speed of the spectrometer can be varied to measure spectra in between 27 ms to 216 ms. Thus, the spectral point spacing and tuning rates span from $\delta\nu = 1.3$ MHz to 160 kHz, and $\dot{\nu} = 380$ GHz/s to 47 GHz/s, respectively, according to Eq. (1). We estimate an accumulated chirp [22] rate of 44 THz/s to 5.6 THz/s, considering 120 lines which sweep in parallel.

At faster rates, the optical comb lines no longer tune continuously. We have previously observed that optical feedback can cause one or both combs to change state, whereby the frequencies and the envelope of the combs suddenly change. This manifests itself in a sudden change in the envelope and/or spacing of the beat note pattern. Slower tuning is possible but requires a larger buffer in the acquisition unit.

Figure 4 displays the statistics in the form of box plots of the retrieved N_2O line centers with respect to literature reference for varying scanning speeds. Scan speeds up to 380 GHz/s do not induce noticeable offsets in the retrieved line centers, within the uncertainties. This shows that delays due to the RF scheme are negligible. Potential delays at faster scanning speeds could be assessed and corrected from a reference measurement.

VI. DISCUSSION

We have demonstrated a fast and accurate midinfrared dual-comb spectrometer. The combs were emitted by quantum cascade lasers, which can be tuned over their free spectral range (f_{rep}) in tens of milliseconds to provide high-resolution spectra of broad molecular bands. We calibrated the frequency axis by measuring the beat between the interrogating comb and a reference laser and by acquiring the comb's repetition rate. Moreover, we have enhanced the marker method [25] using a synthetic comb, to process the fast chirp of the beat between the comb and the reference laser. This method is compatible with other integrated comb technologies featuring multi-GHz repetition frequencies such as microresonator combs [7], and could also be applied to comb-calibrated spectroscopy [25].

Our agile spectrometer provides unique performances in terms of acquisition speed and frequency accuracy compared to other broadband spectrometers with small (<10 MHz) spectral point spacing [15,25,27,29,30]. Indeed, it is faster at acquiring a full spectra than a stepped comb [15,27], and the accumulated chirp, thanks to the parallel scanning of the comb lines, is larger than the chirp commonly used in tunable laser spectroscopy [25,29,30]. Moreover, the adapted marker scheme yields an absolute frequency axis, which allows unambiguous identification of the molecular transitions even with the large chirp. Thus, our spectrometer is a promising candidate toward an on-chip gas sensor that is highly sensitive and selective to many relevant molecules, allowing real-time monitoring of complex gas mixtures at Hz-level refresh rates in industrial processes for example.

Finally, we believe that the spectrometer sensitivity, bandwidth, and power-efficiency will improve thanks to ongoing development in quantum cascade laser frequency combs, such as mutual stabilization [24,31], dispersion management [32], and full spectrometer integration [33].

Data underlying the results presented in this paper are available at the EUDAT B2SHARE repository b2share [34].

ACKNOWLEDGMENTS

We thank Prof. Jérôme Faist and Dr. Mathieu Bertrand at ETH for providing the QCL combs and lending the horn antenna used in this work. We also thank Dr. Stéphane Schilt for fruitful discussions concerning the marker scheme. We acknowledge funding from the Schweizerischer Nationalfonds zur Förderung der Wissenschaftlichen Forschung (Grant No. 40B2-1_176584).

APPENDIX: ADDITIONAL EXPERIMENTAL DETAILS

1. Lasers

The two laser sources were InGaAs/AlInAs on InP-based dual-stack QCLs [17,35]. They were 4.5 mm long ($f_{\mathrm{rep}} \approx 9.88$ GHz, $\Delta f_{\mathrm{rep}} \approx 4.5$ MHz) and had both end facets uncoated. The combs emitted several hundred mW of optical power over $\sim$50 cm^{-1} (1.5 THz) in the 1300 cm^{-1} (39 THz) range [see Fig. 1(b)]. A pair of neutral density filters immediately attenuated the optical power in each beam to approximately 20 mW. Two polarizers in front of the detectors [not shown in Fig. 1(a)] finally attenuated the power to about 0.5 mW. The lasers were operated at constant temperature of 1.9 °C and 2.2 °C, respectively. The combs were electrically driven by a pair of QubeCL drivers (ppqSense). The bias currents for the two combs were 1532 mA and 1226 mA, respectively. The currents were modulated by asymmetric triangular wave forms (WFG1 and WFG2 are the two outputs of an ArbStudio 1102, LeCroy wave form generator) with the currents initially decreasing at constant rate during a time $T = 30$ ms, 60 ms, 120 ms, or 240 ms and returning to the initial value over a shorter time $0.25T$. The peak-to-peak current modulation amplitude was approximately 90 mA for both lasers. This required a modification of the QubeCL drivers which, by default, do not allow such large current modulations.

2. Beam splitters

The beam splitters were custom made to obtain the appropriate power ratios at each photodetector. They were designed for reflecting 1%, 10%, or 50% at an angle of incidence of 45 ° for *s*-polarized light from 1220 to 1370 cm^{-1} (36.6 to 41.1 THz). They were produced by ion beam sputtering (IBS) on 5 mm thick wedged (0.5 °) CaF_2 substrates with an antireflection coating on the back side to minimize undesired interference effects.

3. Data acquisition and processing

Two 1 GHz bandwidth MIR photodetectors were employed to measure the sample (DS) and to normalize laser intensity and phase noise (DN). Each beat note arising from heterodyning of two comb lines appears on both detectors and their amplitudes are measured simultaneously. The division (DS/DN) of the amplitudes yields a ratio in which common-mode fluctuations in magnitude and phase are canceled. The detector outputs were sampled at 2.5 GSa/s with 12 bit resolution by the data acquisition unit DAQ1 (ADQ32, Teledyne), generating 10 Gbyte/s of raw data for the duration of the sweep. The data acquisition was triggered at $t = 0.07T$ after the start of the (decreasing) current ramp and continued for a duration of 27 ms, 54 ms, 107 ms, or 215 ms, which corresponds to 2^{26}, 2^{27}, 2^{28}, or 2^{29} samples at 2.5 GSa/s. The clocks of DAQ1 [Fig. 1(a)] and of the synthesizer generating the 475 MHz fundamental for the synthetic comb generator were referenced to a GPS-disciplined clock (GPSDO, Leo Bodnar).

A custom software (C++ and CUDA) was used to process the two interferograms. The program is capable of fully processing (from raw data to absorbance values) 25 27-ms-long sweeps per second, corresponding to a raw data throughput of 6.75 Gbyte/s, or 67.5% of the maximum raw data input rate. The interferograms were first divided into slices of length $2^{15} = 32\,768$ samples, corresponding to 13.1 µs. The beat note amplitudes were computed for each slice by fast Fourier transform, from which the sample's absorbance was determined.

4. Measurement of the markers and retrieval of the frequency axis

The optical frequency reference, ν_{ref}, was provided by a distributed feedback QCL (DFB, Alpes Lasers) packaged in a TO3 can and emitting a continuous wave (cw) beam. The laser was locked to a molecular transition [N_2O, fundamental ν_1 band, P(14)] by means of a wavelength modulation scheme, in a similar implementation to that in [23]. The wavelength modulation signal at 14 MHz was sent to the laser via a custom-made bias tee. The proportional-integral controller (LB1005-S, Newport) and the laser driver (QCL500 LAB, Wavelength Electronics) assured a locking bandwidth $\geqslant$100 kHz. Diluted N_2O gas flowed through a 15-cm-long custom-made gas cell at a constant pressure of 2 mbar (pressure regulator: PC Series, Alicat).

The lock point frequency was determined relative to the center frequency of the P(14) transition by recording both the error and the transmission signals while slowly tuning the

laser over the transition with the feedback loop open. By comparing the dual-comb spectra with the literature, we observed that the reference laser drifted with a standard deviation on the order of 250 kHz over a few days. We thus made sure to reassess the lock point before each measurement (within 6 hours), leading to the 180 kHz uncertainty of the laser lock point.

The heterodyne beat between the DFB reference laser and COMB1 is detected on the fast photodetector (UHSM-10.6 PV-4TE-10.6-0.05-butt, Vigo System). Through RF path 1, two pulses are transmitted in rapid succession when $f_b(t)$ passes near zero and are amplified by a logarithmic amplifier (ZX47-60LN-S+, Minicircuits). The timings of the two peaks, $t_0^{\pm}$, fulfill $f_b(t_0^{\pm}) = \pm f_{\mathrm{bp},1}$, where $f_{\mathrm{bp},1} = 25$ MHz is the center frequency of BPF1. We assume linear chirping of the beat between t_0^- and t_0^+, so that $f_b(t_0) = 0$, where t_0 is the mean of t_0^+ and t_0^-. With Eq. (2) we find $\nu_0(t_0) = \nu_{\mathrm{ref}}$.

As for RF path 2, $f_b(t)$ is mixed with an RF comb with spacing f_{RF}. Therefore, each time the DFB-comb beat, $f_b(t)$, nears a multiple of f_{RF}, two double pulses are recorded on channels 2 and 3 of DAQ2 [signal 2 and signal 3 in Figs. 2(a) and 2(b)]. The timings, $t_n^{\pm}$, of the two pulses of the nth ($n = \pm1, \pm2, \ldots$) double pulse fulfill $f_b(t_n^{\pm}) = nf_{\mathrm{RF}} \pm f_{\mathrm{bp,i}}$, where $f_{\mathrm{bp},2} = 21$ MHz, $f_{\mathrm{bp},3} = 45$ MHz are the center frequencies of BPF2 and BPF3, respectively. For the mean times, $t_n = (t_n^- + t_n^+)/2$, we find, as before, $f_b(t_n) = nf_{\mathrm{RF}}$ and with Eq. (2), $\nu_0(t_n) = \nu_{\mathrm{ref}} + nf_{\mathrm{RF}}$. More details concerning the processing of the markers can be found in Fig. 1 and Note 1 of the Supplemental Material [26].

As postprocessing, we first smooth the marker signals with a low-pass filter. Then we detect the peaks which match specific criteria in terms of prominence, width, and proximity to other lines using a peak-finding algorithm (find_peaks, scipy). If two peaks have the appropriate time delay, we establish that f_b was at a multiple integer n of f_{RF} at the mean time of the two peaks. The integer n is guessed from linear interpolation using marker 1 and an estimated chirp. The discontinuity from the change of comb line can be easily recognized and the markers originating from comb line $\mu = 1$ can be used to determine the frequency of comb line $\mu = 0$ by knowledge of $f_{\mathrm{rep}}(t)$.

We fit the markers with polynomials of increasing orders up to 10, keeping the coefficients of the previous order as initial guess and providing the initial guess for the new coefficient from the residuals of the previous fit. A larger weight is given to marker 2 as BPF2 is narrower than the other bandpass filters. After the fits with the 4th and 8th order polynomial, markers outside a tolerance of 50 MHz and 10 MHz are discarded, respectively. This allows the removal of most spurious peaks, which do not align in the plot Fig. 2(d).

5. Measurement of the repetition rate

In QCL frequency combs, the beating of all co-existing modes in the laser produces a measurable voltage modulation on the laser electrodes with frequency equal to f_{rep} [36]. The laser module features a 50 Ω transmission line on a printed circuit board that connects an SMA connector at the back of the housing to a point very close (within 1 mm) to the back facet of the laser. From there, a short bond wire establishes an electrical connection to the laser's top electrode. This pathway can be used for RF injection or to measure f_{rep}. However, connecting cables and other circuitry to the SMA port tends to increase laser phase noise. It is observable as a broadening of the beat notes. Therefore, a horn antenna (ANT, PowerLOG 40040, Aaronia) was pointed at the open SMA connector. The detected f_{rep} was then amplified and down-mixed to ∼20 MHz to enable its measurement on one channel of DAQ1.

6. Gas sample preparation and measurement

We dynamically diluted N_2O gas with nitrogen to a concentration of about of 450 ppmv and flowed the diluted mixture through the multipass cell (MPC). We then closed off the cell and pumped down to 1.5 mbar, which provided sufficiently strong absorption lines and sufficiently low pressure to be reasonably close to the Doppler-broadened limit and, more importantly, to minimize the pressure-induced shift on the measured transitions. Multiple sweeps were taken but not averaged together. The time delay between sweeps was several seconds, to ensure proper synchronization of the two data sets acquired by the two DAQs, which were read out by independent software. By integrating both DAQs in the same processing routine, the acquisition rate (sweeps per unit time) could be increased significantly (about 12 54-ms-long sweeps per second).

[1] F. Keilmann, C. Gohle, and R. Holzwarth, Time-domain mid-infrared frequency-comb spectrometer, Opt. Lett. **29**, 1542 (2004).

[2] I. Coddington, N. Newbury, and W. Swann, Dual-comb spectroscopy, Optica **3**, 414 (2016).

[3] F. R. Giorgetta, J. Peischl, D. I. Herman, G. Ycas, I. Coddington, N. R. Newbury, and K. C. Cossel, Open-path dual-comb spectroscopy for multispecies trace gas detection in the 4.5–5 μm spectral region, Laser Photonics Rev. **15**, 2000583 (2021).

[4] J. L. Klocke, M. Mangold, P. Allmendinger, A. Hugi, M. Geiser, P. Jouy, J. Faist, and T. Kottke, Single-shot sub-microsecond mid-infrared spectroscopy on protein reactions with quantum cascade laser frequency combs, Anal. Chem. **90**, 10494 (2018).

[5] E. Vicentini, Z. Wang, K. Van Gasse, T. W. Hänsch, and N. Picqué, Dual-comb hyperspectral digital holography, Nat. Photonics **15**, 890 (2021).

[6] A. Parriaux, K. Hammani, C. Thomazo, O. Musset, and G. Millot, Isotope ratio dual-comb spectrometer, Phys. Rev. Res. **4**, 023098 (2022).

[7] T. J. Kippenberg, A. L. Gaeta, M. Lipson, and M. L. Gorodetsky, Dissipative Kerr solitons in optical microresonators, Science **361**, eaan8083 (2018).

[8] A. Hugi, G. Villares, S. Blaser, H. C. Liu, and J. Faist, Mid-infrared frequency comb based on a quantum cascade laser, Nature (London) **492**, 229 (2012).

[9] M. Bagheri, C. Frez, L. A. Sterczewski, I. Gruidin, M. Fradet, I. Vurgaftman, C. L. Canedy, W. W. Bewley, C. D. Merritt,

C. S. Kim, M. Kim, and J. R. Meyer, Passively mode-locked interband cascade optical frequency combs, Sci. Rep. **8**, 3322 (2018).

[10] Y.-D. Hsieh, Y. Iyonaga, Y. Sakaguchi, S. Yokoyama, H. Inaba, K. Minoshima, F. Hindle, T. Araki, and T. Yasui, Spectrally interleaved, comb-mode-resolved spectroscopy using swept dual terahertz combs, Sci. Rep. **4**, 3816 (2014).

[11] G. Villares, A. Hugi, S. Blaser, and J. Faist, Dual-comb spectroscopy based on quantum-cascade-laser frequency combs, Nat. Commun. **5**, 5192 (2014).

[12] A. V. Muraviev, D. Konnov, and K. L. Vodopyanov, Broadband high-resolution molecular spectroscopy with interleaved mid-infrared frequency combs, Sci. Rep. **10**, 18700 (2020).

[13] P.-L. Luo, Long-wave mid-infrared time-resolved dual-comb spectroscopy of short-lived intermediates, Opt. Lett. **45**, 6791 (2020).

[14] T. Lin, A. Dutt, C. Joshi, X. Ji, C. T. Phare, Y. Okawachi, A. L. Gaeta, and M. Lipson, Broadband ultrahigh-resolution chip-scale scanning soliton dual-comb spectroscopy, arXiv:2001.00869.

[15] A. Hjältén, M. Germann, K. Krzempek, A. Hudzikowski, A. Głuszek, D. Tomaszewska, G. Soboń, and A. Foltynowicz, Optical frequency comb Fourier transform spectroscopy of $^{14}N_2{}^{16}O$ at 7.8 μm, J. Quant. Spectrosc. Radiat. Transfer **271**, 107734 (2021).

[16] M. Lepère, O. Browet, J. Clément, B. Vispoel, P. Allmendinger, J. Hayden, F. Eigenmann, A. Hugi, and M. Mangold, A mid-infrared dual-comb spectrometer in step-sweep mode for high-resolution molecular spectroscopy, J. Quant. Spectrosc. Radiat. Transfer **287**, 108239 (2022).

[17] M. Gianella, A. Nataraj, B. Tuzson, P. Jouy, F. Kapsalidis, M. Beck, M. Mangold, A. Hugi, J. Faist, and L. Emmenegger, High-resolution and gapless dual comb spectroscopy with current-tuned quantum cascade lasers, Opt. Express **28**, 6197 (2020).

[18] N. Kuse, G. Navickaite, M. Geiselmann, T. Yasui, and K. Minoshima, Frequency-scanned microresonator soliton comb with tracking of the frequency of all comb modes, Opt. Lett. **46**, 3400 (2021).

[19] E. Benkler, F. Rohde, and H. R. Telle, Endless frequency shifting of optical frequency comb lines, Opt. Express **21**, 5793 (2013).

[20] M. Gianella, S. Vogel, V. J. Wittwer, T. Südmeyer, J. Faist, and L. Emmenegger, Frequency axis for swept dual-comb spectroscopy with quantum cascade lasers, Opt. Lett. **47**, 625 (2022).

[21] M. Germann, A. Hjältén, V. Boudon, C. Richard, K. Krzempek, A. Hudzikowski, A. Głuszek, G. Soboń, and A. Foltynowicz, A methane line list with sub-MHz accuracy in the 1250 to 1380 cm^{-1} range from optical frequency comb Fourier transform spectroscopy, J. Quant. Spectrosc. Radiat. Transfer **288**, 108252 (2022).

[22] J. Riemensberger, A. Lukashchuk, M. Karpov, W. Weng, E. Lucas, J. Liu, and T. J. Kippenberg, Massively parallel coherent laser ranging using a soliton microcomb, Nature (London) **581**, 164 (2020).

[23] K. N. Komagata, M. Gianella, P. Jouy, F. Kapsalidis, M. Shahmohammadi, M. Beck, R. Matthey, V. J. Wittwer, A. Hugi, J. Faist, L. Emmenegger, T. Südmeyer, and S. Schilt, Absolute frequency referencing in the long wave infrared using a quantum cascade laser frequency comb, Opt. Express **30**, 12891 (2022).

[24] K. Komagata, A. Shehzad, G. Terrasanta, P. Brochard, R. Matthey, M. Gianella, P. Jouy, F. Kapsalidis, M. Shahmohammadi, M. Beck, V. J. Wittwer, J. Faist, L. Emmenegger, T. Südmeyer, A. Hugi, and S. Schilt, Coherently-averaged dual comb spectrometer at 7.7 μm with master and follower quantum cascade lasers, Opt. Express **29**, 19126 (2021).

[25] P. Del'Haye, O. Arcizet, M. L. Gorodetsky, R. Holzwarth, and T. J. Kippenberg, Frequency comb assisted diode laser spectroscopy for measurement of microcavity dispersion, Nat. Photonics **3**, 529 (2009).

[26] See Supplemental Material at http://link.aps.org/supplemental/10.1103/PhysRevResearch.5.013047 for more information on the processing of the markers and the measured methane line list.

[27] B. AlSaif, M. Lamperti, D. Gatti, P. Laporta, M. Fermann, A. Farooq, O. Lyulin, A. Campargue, and M. Marangoni, High accuracy line positions of the ν_1 fundamental band of $^{14}N_2{}^{16}O$, J. Quant. Spectrosc. Radiat. Transfer **211**, 172 (2018).

[28] I. Gordon, L. Rothman, R. Hargreaves, R. Hashemi, E. Karlovets, F. Skinner, E. Conway, C. Hill, R. Kochanov, Y. Tan, P. Wcisło, A. Finenko, K. Nelson, P. Bernath, M. Birk, V. Boudon, A. Campargue, K. Chance, A. Coustenis, B. Drouin *et al.*, The HITRAN2020 molecular spectroscopic database, J. Quant. Spectrosc. Radiat. Transfer **277**, 107949 (2022).

[29] A. Nishiyama, D. Ishikawa, and M. Misono, High resolution molecular spectroscopic system assisted by an optical frequency comb, J. Opt. Soc. Am. B **30**, 2107 (2013).

[30] R. Gotti, T. Puppe, Y. Mayzlin, J. Robinson-Tait, S. Wójtewicz, D. Gatti, B. Alsaif, M. Lamperti, P. Laporta, F. Rohde, R. Wilk, P. Leisching, W. G. Kaenders, and M. Marangoni, Comb-locked frequency-swept synthesizer for high precision broadband spectroscopy, Sci. Rep. **10**, 2523 (2020).

[31] J. Hillbrand, M. Bertrand, V. Wittwer, N. Opacak, F. Kapsalidis, M. Gianella, L. Emmenegger, B. Schwarz, T. Südmeyer, M. Beck, and J. Faist, Synchronization of frequency combs by optical injection, Opt. Express **30**, 36087 (2022).

[32] G. Villares, S. Riedi, J. Wolf, D. Kazakov, M. J. Süess, P. Jouy, M. Beck, and J. Faist, Dispersion engineering of quantum cascade laser frequency combs, Optica **3**, 252 (2016).

[33] B. Schwarz, P. Reininger, D. Ristanić, H. Detz, A. M. Andrews, W. Schrenk, and G. Strasser, Monolithically integrated mid-infrared lab-on-a-chip using plasmonics and quantum cascade structures, Nat. Commun. **5**, 4085 (2014).

[34] K. N. Komagata, V. J. Wittwer, T. Südmeyer, L. Emmenegger, and M. Gianella, Data set for "Absolute frequency referencing for swept dual-comb spectroscopy with midinfrared quantum cascade lasers", https://doi.org/10.23728/b2share.2a4682099b614b38b90952e42b8a425f (2022).

[35] P. Jouy, J. M. Wolf, Y. Bidaux, P. Allmendinger, M. Mangold, M. Beck, and J. Faist, Dual comb operation of $\lambda \sim 8.2$ μm quantum cascade laser frequency comb with 1 W optical power, Appl. Phys. Lett. **111**, 141102 (2017).

[36] M. Piccardo, D. Kazakov, N. A. Rubin, P. Chevalier, Y. Wang, F. Xie, K. Lascola, A. Belyanin, and F. Capasso, Time-dependent population inversion gratings in laser frequency combs, Optica **5**, 475 (2018).